

# Deceleration and electrostatic trapping of OH radicals

Sebastiaan Y.T. van de Meerakker,<sup>1,2</sup> Paul H.M. Smeets,<sup>2</sup> Nicolas Vanhaecke,<sup>1</sup> Rienk T. Jongma,<sup>3</sup> and Gerard Meijer<sup>1</sup>

<sup>1</sup>*Fritz-Haber-Institut der Max-Planck-Gesellschaft, Faradayweg 4-6, 14195 Berlin, Germany*

<sup>2</sup>*FOM-Institute for Plasmaphysics Rijnhuizen, Edisonbaan 14, 3439 MN Nieuwegein, The Netherlands*

<sup>3</sup>*Space Research Organization Netherlands, Sorbonnelaan 2, 3584 CA Utrecht, The Netherlands*

(Dated: November 19, 2018)

A pulsed beam of ground state OH radicals is slowed down using a Stark decelerator and is subsequently loaded into an electrostatic trap. Characterization of the molecular beam production, deceleration and trap loading process is performed via laser induced fluorescence detection inside the quadrupole trap. Depending on details of the trap loading sequence, typically  $10^5$  OH ( $X^2\Pi_{3/2}, J = 3/2$ ) radicals are trapped at a density of around  $10^7$  cm<sup>-3</sup> and at temperatures in the 50-500 mK range. The  $1/e$  trap lifetime is around 1.0 second.

PACS numbers: 33.80.Ps, 33.55.Be, 39.10.+j

Getting ever better control over both the internal and external degrees of freedom of gas-phase molecules has been an important theme in molecular physics during the last decades. This control is important, for instance, in spectroscopic investigations, in collision and reactive scattering experiments and in photo-dissociation, or half-collision, studies. Seeded molecular beams, both continuous and pulsed, have been extensively used to produce samples of molecules in only the lowest internal energy states, with typical rotational temperatures of a few K [1]. In these molecular beams the longitudinal velocity distribution is also well defined, and translational temperatures of around 1 K are obtained in the moving frame of the molecular beam. Further control over the molecules is achieved when their orientation in space is actively manipulated, using either static electro-magnetic fields and/or radiation fields [2]. Sophisticated and powerful detection schemes have been developed to experimentally study (half-) collisions [3, 4] and reactions [5] of the thus prepared molecules in the required detail.

Over the last years our group has been developing methods to get improved control over the absolute velocity and over the velocity spread of molecules in a molecular beam [6]. These methods rely on the, quantum-state specific, force that polar molecules experience in electric fields. This force is rather weak, typically some eight to ten orders of magnitude weaker than the force that the corresponding molecular ion experiences in the same electric field. This force nevertheless suffices to achieve complete control over the motion of polar molecules, using techniques akin to those used for the control of charged particles. We have explicitly demonstrated this by the construction of two types of linear accelerators [7], a buncher [8], a trap [9] and a storage ring [10] for neutral polar molecules. Using these tools, state-selected molecular beams with a computer-controlled absolute velocity and with record-low (longitudinal) temperatures have been produced. This holds great promise for the use of decelerated molecular beams in metrology, i.e., in experiments aimed at testing fundamental symmetries [11].

To be able to exploit the possibilities that these new tools offer for collision and reactive scattering experiments, the fraction of the pulsed molecular beam that is decelerated and/or trapped needs to come closer to unity, i.e., the 6-dimensional phase space acceptance of the various elements needs to be increased to better match to the typical emittance of a molecular beam. In addition, deceleration and trapping needs to be performed on those molecules that are of most relevance in collision and reactive scattering experiments; thus far, electrostatic trapping after Stark deceleration has only been demonstrated for ND<sub>3</sub> molecules [9, 12].

We here report the deceleration and electrostatic trapping of ground state OH ( $X^2\Pi_{3/2}, J = 3/2$ ) radicals. The experiments are performed in a new generation molecular beam deceleration machine, designed such that a large fraction of the molecular beam pulse can be slowed down and trapped. The role of the omnipresent OH radical as intermediate in many chemical reactions has made this a benchmark molecule in collision and reactive scattering studies. Hexapole state-selection and focusing, e.g., transverse phase space manipulation, of a beam of OH is well documented and often used in these studies [13]. The possibility to manipulate the longitudinal phase-space distribution of OH radicals inside a decelerator has recently been demonstrated as well [14].

The experimental setup is schematically shown in Fig. 1. A pulsed beam of OH with a mean velocity of 460 m/s and with a velocity spread of 15 % (full width half maximum, FWHM) is produced via ArF-laser dissociation of HNO<sub>3</sub> seeded in Kr near the orifice of a pulsed valve. Production thus takes place at a well-defined time and at a well-defined position, which is ideal for coupling the molecular beam into the decelerator. More than 95 % of the OH radicals in the beam reside in the lowest rotational and vibrational level of the  $X^2\Pi_{3/2}$  spin-orbit manifold of the electronic ground state. This population is distributed over the two  $\Lambda$ -doublet components of the  $J = 3/2$  level, which has a zero-field splitting of  $0.055$  cm<sup>-1</sup>. Only OH radicals in low-field seeking quan-

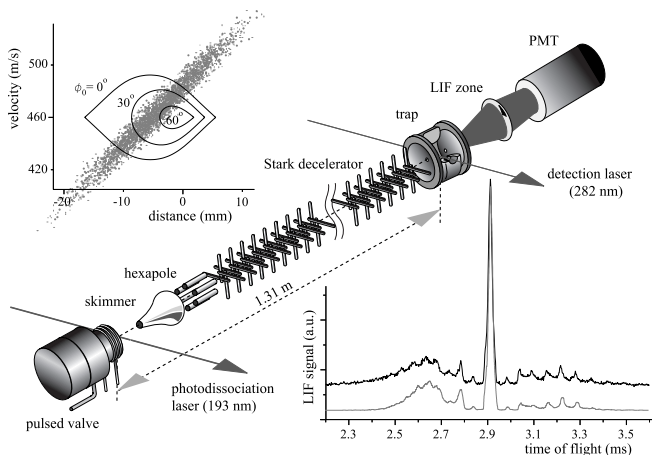


FIG. 1: Scheme of the experimental setup. The longitudinal phase space acceptance of the decelerator for OH ( $J = 3/2, |M_J\Omega| = 9/4$ ) is given for three different phase angles  $\phi_0$ , together with the longitudinal phase space distribution of the OH beam at the entrance of the decelerator (shaded area). The observed LIF signal as a function of time after OH production with the decelerator operating at  $\phi_0 = 0^\circ$  (upper curve) is shown together with a simulation (lower curve).

tum states, i.e., radicals in the upper  $\Lambda$ -doublet component which splits into  $|M_J\Omega| = 3/4$  and  $|M_J\Omega| = 9/4$  components in an electric field, are of relevance in this experiment. The force that the OH radicals experience in electric fields is, in the linear regime, proportional to  $|M_J\Omega|$ . Only molecules in (both  $|M_F|$  hyperfine sublevels of) the  $J = 3/2, |M_J\Omega| = 9/4$  component are therefore decelerated and trapped in the present experiments, although molecules in both  $|M_J\Omega|$  components contribute to the laser induced fluorescence (LIF) signal of the non-decelerated beam that is passing through the trap.

After passage through a 2 mm diameter skimmer, the molecular beam enters the deceleration chamber and is focussed into the Stark decelerator by a short hexapole. The hexapole matches the transverse phase space distribution of the OH ( $J = 3/2, |M_J\Omega| = 9/4$ ) radicals at the entrance of the decelerator to the transverse acceptance of the decelerator. A detailed description of the operation principle of a Stark decelerator and an electrostatic quadrupole trap, as well as of (the importance of) phase-space matching between the various elements in the molecular decelerator beam-line is given elsewhere [12]. In the current design the dimensions of the decelerator are scaled up by a factor of two relative to earlier designs. With the electric field stages in the decelerator now at a distance of 11 mm, and with a  $4 \times 4$  mm<sup>2</sup> transverse acceptance area between the two 6 mm diameter parallel electrodes that make up one electric field stage, the total spatial acceptance of the decelerator has been increased by a factor eight. This upscaling has been performed while maintaining the same electric field strength inside the decelerator; in the present ex-

periments a voltage difference of 40 kV is switched on and off in an electric field stage. The area within the outer contour in the upper left corner in Fig. 1 is the thus obtained longitudinal acceptance of the decelerator for phase-stable transport of OH ( $J = 3/2, |M_J\Omega| = 9/4$ ) without deceleration. With a distance from the source to the decelerator of only about 10 cm, this longitudinal acceptance largely encompasses the longitudinal emittance of the pulsed OH beam, indicated by the shaded area. When operating the decelerator at  $\phi_0 = 0^\circ$  for a synchronous molecule with a velocity of 450 m/s, a time of flight (TOF) profile of the OH ( $J = 3/2$ ) radicals exiting the decelerator as shown in the lower right corner of Fig. 1 is observed. The main portion of the OH beam is transported through the machine as a compact package (less than  $25 \mu\text{s}$  FWHM in the TOF profile), independent of the length of the decelerator. The TOF profile resulting from a three-dimensional trajectory calculation, shown underneath the measurement, quantitatively reproduces the observation. From the calculations, the contributions of the individual  $|M_J\Omega|$  components to the TOF profile can be identified. In addition, these calculations enable a detailed understanding of the untrapped dynamics in the decelerator, which manifests itself by the features in the wings of the observed TOF profile.

For deceleration of the molecular beam, operation at a phase angle  $0^\circ < \phi_0 < 90^\circ$  is required. As the longitudinal acceptance of the decelerator rapidly decreases with increasing phase angle it is often advantageous to operate the decelerator at a relatively low phase angle, i.e., to extract a smaller amount of energy from the molecular beam per deceleration stage, and to use more deceleration stages instead. The decelerator used in the current experiment consists out of 108 deceleration stages, and has a length of 1188 mm. The large number of deceleration stages also enables the deceleration of molecular beams with a higher initial velocity; in the present experiment this enables the use of Kr for seeding instead of Xe, which reduces cluster formation in the expansion. In experiments that we have performed to produce decelerated beams of metastable NH radicals, it was unfavorable to use Xe as a carrier gas as it efficiently quenches the electronically excited species. Only by performing 266 nm dissociation of  $\text{HN}_3$  seeded in Kr a sufficiently intense beam of NH ( $a^1\Delta, J = 2$ ) radicals could be produced, which we have subsequently decelerated from 550 m/s to 330 m/s (data not shown).

The electrostatic trap consists of a ring electrode, centered 21 mm downstream from the last electrodes of the decelerator, with an inner radius  $R$  of 10 mm and two hyperbolic end-caps with a half-spacing of  $R/\sqrt{2}$ . This trap is scaled up by a factor two compared to the trap that we have used thus far [12]. The molecular beam enters the trap through a 4 mm diameter hole in the first end-cap. This hole is the only vacuum connection between the deceleration chamber and the trap chamber,

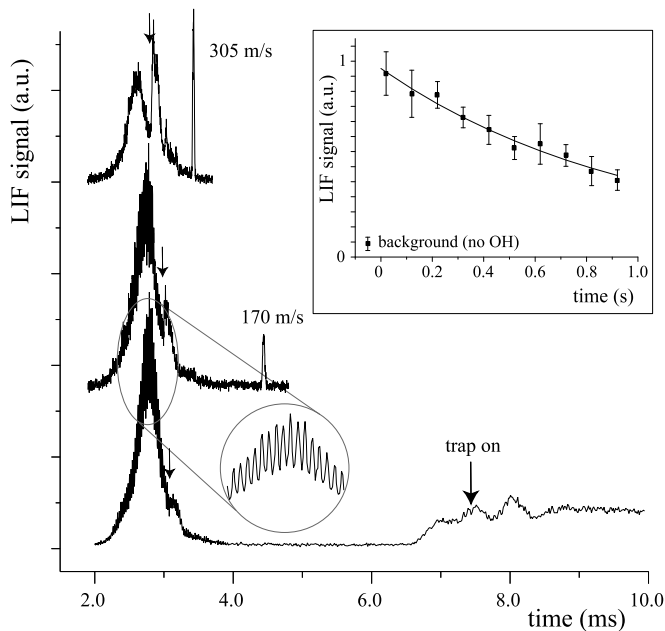


FIG. 2: LIF signal of OH ( $J = 3/2$ ) radicals at the center of the quadrupole trap as a function of time after OH production for two different deceleration sequences (upper two curves) and for a deceleration and trapping sequence (lower curve). In the inset, the LIF signal intensity of the electrostatically trapped OH radicals is shown on a longer time-scale.

and the pressure in the trap chamber can be kept at  $5 \times 10^{-9}$  mbar under operating conditions. Optical access to the trap is provided by two 6 mm diameter holes in the ring electrode. The beam of a frequency doubled pulsed dye laser is sent through these holes to perform LIF detection of the OH radicals at the center of the trap. Excitation is performed on the  $Q_1(1)$  transition of the  $A^2\Sigma^+, v = 1 \leftarrow X^2\Pi_{3/2}, v = 0$  band around 282 nm, selectively detecting OH ( $J = 3/2$ ) radicals in the upper  $\Lambda$ -doublet component. Off-resonant fluorescence on the  $A^2\Sigma^+, v = 1 \rightarrow X^2\Pi, v = 1$  band around 313 nm is imaged through a 6 mm diameter opening in the second end-cap onto a photomultiplier tube (PMT). Stray light from the laser is largely avoided by using light baffles and is suppressed by optical filtering in front of the PMT.

In Fig. 2 the intensity of the LIF signal of OH ( $J = 3/2$ ) radicals at the center of the trap is shown as a function of time after firing the dissociation laser, using different deceleration and trap loading sequences. In the measurement shown in the upper curve, the decelerator is operated at a phase angle of  $\phi_0 = 50^\circ$ , extracting about  $0.9 \text{ cm}^{-1}$  of kinetic energy from the synchronous molecule in every deceleration stage; OH radicals with an initial velocity of around 465 m/s are decelerated to a final velocity of around 305 m/s. Due to a better spatial confinement, the peak density of the decelerated portion of the molecular beam is higher than the peak density of the non-decelerated beam that passes through the trap.

The hole in the TOF profile of the fast beam due to the disappearance of OH radicals that are decelerated is indicated by an arrow. In the measurement shown in the middle curve, OH radicals with an initial velocity around 440 m/s are decelerated to 170 m/s, operating the decelerator at a phase angle of  $\phi_0 = 70^\circ$ . In the lower curve, the observed TOF profile is shown when the decelerator operates at  $\phi_0 = 77^\circ$ , extracting about  $1.2 \text{ cm}^{-1}$  of kinetic energy per deceleration stage. OH radicals with an initial velocity of 428 m/s ( $E_{kin} = 130 \text{ cm}^{-1}$ ) exit the decelerator with a velocity of around 21 m/s. The OH radicals in the non-decelerated part of the beam also experience the switched electric fields inside the decelerator. This leads to a highly structured phase-space distribution and results in rich oscillatory structure on the TOF profile of the fast beam, as shown enlarged in the figure. The slow beam of OH radicals is loaded into the electrostatic trap with voltages of 7 kV, 15 kV and -15 kV on the first end-cap, the ring electrode and the second end-cap, respectively. This creates a potential hill in the trap that is higher than the remaining kinetic energy of the molecules. The OH radicals therefore come to a standstill near the center of the trap, around 7.4 ms after their production. At that time, indicated by an arrow in Fig. 2, the first end-cap is switched from 7 kV to -15 kV to create a (nearly) symmetric 500 mK deep potential well. After some initial oscillations, a steady LIF signal is observed from the OH radicals in the trap. The LIF intensity of the trapped OH radicals is about 20 % of the peak LIF intensity of the non-decelerated beam of OH that passes through the trap. The observed LIF signal of the trapped OH radicals corresponds to a total number of about  $10^5$  OH ( $J = 3/2, |M_J/\Omega| = 9/4$ ) radicals, in the approximately  $0.03 \text{ cm}^3$  detection volume in the trap. In the inset, the LIF signal intensity is shown on a longer time-scale, from which a  $1/e$  trap lifetime on the order of 1.0 second, limited by collisions with background gas, is deduced.

The absolute number of OH radicals that can be trapped as well as the phase space distribution of the trapped molecules critically depends on the details of the trap loading sequence. In Fig. 3 measurements are shown for two slightly different trap trap loading conditions, referred to as case A and case B. Curve A(i) and B(i) show the TOF profile of the slow beam of OH radicals that passes through the trap when no voltages are applied to the trap electrodes. Due to the lower beam velocity of around 15 m/s in case B compared to the 21 m/s in case A, the beam arrives later at the center of the trap, is spread out more and has a lower peak density. Curve A(ii) and B(ii) show the TOF profile when the voltages for trap loading as given earlier are constantly applied to the trap electrodes. In case A the molecules enter the trap too fast, and move past the center of the trap; the observed double-hump structure in the TOF profile is to be interpreted as the signal from both the incom-

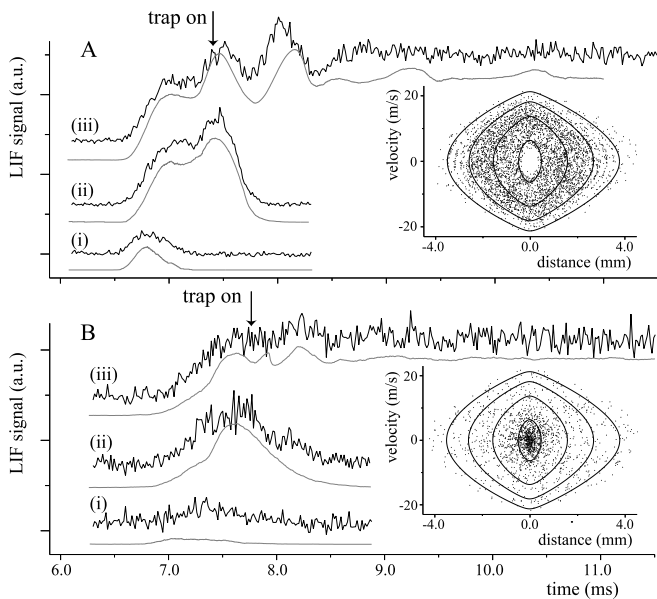


FIG. 3: LIF signal of OH ( $J = 3/2$ ) radicals at the center of the trap as a function of time after OH production for two different trap loading sequences (case A and B), together with the numerically simulated curves. The calculated longitudinal phase space distribution of the OH radicals in the trap at  $t = 30$  ms is shown for both cases.

ing and the reflected beam. In case B the molecules are reflected almost exactly at the center of the trap. Curve A(iii) (identical to the lower curve in Fig. 2) and B(iii) show the resulting TOF profile when we switch from the loading geometry to the trapping geometry at the time indicated by the arrow. The higher initial velocity in case A leads to approximately a factor three more molecules in the trap, but also results in clear oscillations in the TOF profile. When the molecules are (more) correctly coupled into the trap, as in case B, hardly any oscillations are observed. The simulations underneath the experimental data accurately reproduce the observed TOF profiles. The calculated longitudinal phase space distribution of the molecules in the trap at  $t = 30$  ms, shown in Fig. 3 for both cases, should therefore also be realistic. From this, the FWHM of the velocity distribution of the trapped molecules is deduced to be around 30 m/s in case A and around 10 m/s in case B, corresponding to a temperature of 450 mK and 50 mK for the trapped OH radicals, respectively. The density is rather similar in both cases, and is about  $10^7$  cm $^{-3}$ .

The samples of electrostatically trapped OH radicals produced here, are, for instance, ideally suited to investigate the predicted linking of ultracold polar molecules [15]. The experiments reported here are performed in

a molecular beam deceleration and trapping machine that is designed such that almost the complete molecular beam pulse that passes through the skimmer in the right quantum-state can be transported through the trap at a tunable absolute velocity while staying together as a compact package. Alternatively, a sizeable fraction of this molecular beam pulse can be slowed down to a near standstill and loaded into the electrostatic trap, where the molecules can then be trapped up to seconds. Sensitive quantum-state specific detection of the molecules can be performed inside the quadrupole trap. As the molecular beam machine typically runs at a 10 Hz repetition rate, and as different high voltage switching sequences can be applied to adjacent molecular beam pulses, this together offers the unique possibility to perform "in-beam" collision and reactive scattering experiments as a function of the continuously tunable collision energy and with an unprecedented energy resolution.

This work is part of the research program of the 'Stichting voor Fundamenteel Onderzoek der Materie (FOM)', which is financially supported by the 'Nederlandse Organisatie voor Wetenschappelijk Onderzoek (NWO)'. This work is supported by the EU "Cold Molecules" network and by a fellowship (for R.T.J.) of the Royal Netherlands Academy of Arts and Sciences.

- 
- [1] G. Scoles, ed., *Atomic and Molecular Beam Methods*, Volume 1 & 2, Oxford University Press, New York, (1988) & (1992).
  - [2] H. Stapelfeldt and T. Seideman, *Rev. Mod. Phys.* **75**, 543 (2003).
  - [3] H. Sato, *Chem. Rev.* **101**, 2687 (2001).
  - [4] T.P. Rakitzis, A.J. van den Brom, and M.H.M. Janssen, *Science* **303**, 1852 (2004).
  - [5] K. Liu, *Ann. Rev. Phys. Chem.* **52**, 139 (2001); J.J. Lin *et al.*, *Science* **300**, 955 (2003).
  - [6] H.L. Bethlem and G. Meijer, *Int. Rev. Phys. Chem.* **22**, 73 (2003).
  - [7] H.L. Bethlem, G. Berden, and G. Meijer, *Phys. Rev. Lett.* **83**, 1558 (1999); H.L. Bethlem *et al.*, *Phys. Rev. Lett.* **88**, 133003 (2002).
  - [8] F.M.H. Cromptoets *et al.*, *Phys. Rev. Lett.* **89**, 093004 (2002).
  - [9] H.L. Bethlem *et al.*, *Nature (London)* **406**, 491 (2000).
  - [10] F.M.H. Cromptoets *et al.*, *Nature (London)* **411**, 174 (2001).
  - [11] M.R. Tarbutt *et al.*, *Phys. Rev. Lett.* **92**, 173002 (2004).
  - [12] H.L. Bethlem *et al.*, *Phys. Rev. A* **65**, 053416 (2002).
  - [13] M.C. van Beek *et al.*, *Phys. Rev. Lett.* **86**, 4001 (2001).
  - [14] J.R. Bochinski *et al.*, *Phys. Rev. Lett.* **91**, 243001 (2003).
  - [15] A.V. Avdeenkov and J.L. Bohn, *Phys. Rev. Lett.* **90**, 043006 (2003).